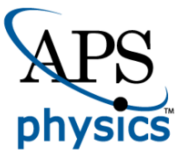

General-relativistic simulations of binary black hole-neutron stars: Precursor electromagnetic signals

Vasileios Paschalidis, Zachariah B. Etienne, and Stuart L. Shapiro

Phys. Rev. D **88**, 021504 — Published 9 July 2013

DOI: 10.1103/PhysRevD.88.021504

General relativistic simulations of binary black hole-neutron stars: Precursor electromagnetic signals

Vasileios Paschalidis, Zachariah B. Etienne, and Stuart L. Shapiro*
Department of Physics, University of Illinois at Urbana-Champaign, Urbana, IL 61801

We perform the first general relativistic force-free simulations of neutron star magnetospheres in orbit about spinning and non-spinning black holes. We find promising precursor electromagnetic emission: typical Poynting luminosities at, e.g., an orbital separation of $r = 6.6R_{\rm NS}$ are $L_{\rm EM} \sim 6 \times 10^{42}(B_{\rm NS,p}/10^{13}{\rm G})^2({\rm M_{NS}}/1.4{\rm M_\odot})^2{\rm erg/s}$. The Poynting flux peaks within a broad beam of $\sim 40^\circ$ in the azimuthal direction and within $\sim 60^\circ$ from the orbital plane, establishing a possible lighthouse effect. Our calculations, though preliminary, preview more detailed simulations of these systems that we plan to perform in the future.

PACS numbers: 04.25.D-,04.25.dk,04.30.-w,52.35.Hr

Black hole–neutron star (BHNS) binaries are promising sources for the simultaneous detection of gravitational wave (GW) and electromagnetic (EM) signals in the era of multimessenger astronomy. For example, aLIGO is expected to detect between 1–100 BHNS GW signals each year [1–4]. Furthermore, BHNS mergers may provide the central engine powering a short-hard gamma-ray burst (sGRB). GW signals from the inspiral and merger of BHNSs were computed recently in full general relativity (GR) [5–11], and the first parametric study of magnetized BHNS mergers in full GR has been carried out in [12, 13], where it was shown that under appropriate conditions BHNSs can launch collimated jets – necessary ingredients for many sGRB models.

Detecting pre-merger EM signals, combined with GW observations, will yield a wealth of information about BHNS binaries. EM signals will help localize the source on the sky, resulting in improved parameter estimation from GWs [14].

Neutron stars likely possess dipole magnetic fields and a force-free magnetosphere [15]. Toward the end of a BHNS inspiral, strong magnetic fields will sweep the BH, possibly establishing a unipolar inductor (UI) that extracts energy from the system [16, 17]. This exciting new possibility has been suggested recently as a potential mechanism for powering precursor EM signals from BHNSs [18]. Follow-up analytical approximations in the high-mass-ratio limit have been performed [19, 20] to estimate the output power. But, as these UIs operate in strongly-curved, dynamical spacetimes, numerical relativity simulations are necessary to reliably determine the amount of EM output, particularly in the regime of comparable-mass binaries where previous approximations do not apply. While UIs may also exist in NSNS binaries [19, 21, 22, 24], BHNSs may be optimal systems for this mechanism because the azimuthal twist (ζ_ϕ) of the magnetic flux tubes is less than unity for a BH resistor [23].

In this Letter we simulate NS magnetospheres in orbit about spinning and nonspinning BHs prior to merger via general relativistic, force-free (GRFF) simulations. We calculate the Poynting luminosity and characterize its angular dependence. We also treat another EM emission mechanism: magnetic dipole (MD) radiation from the accelerating NS. MD radiation has been considered in the context of EM emission affecting the inspiral and GW signal [25], but not as a source for strong precursor EM signals. Here we show that the MD Poynting luminosity is significant, and may dominate the EM output in cases where UI ceases due to corotation or $\zeta_\phi > 1$. We use geometrized units where $c = 1 = G$, unless otherwise stated.

Solving the GRFF equations generally involves evolving the electric ($\mathbf{E}$) and magnetic ($\mathbf{B}$) fields under the force-free constraints $\mathbf{E}\cdot\mathbf{B} = 0$ and $E^2 < B^2$ [26, 27]. The force-free regime represents the limit of ideal MHD when the magnetic fields dominate the plasma dynamics [26, 28]. In this regime, one can choose the $\mathbf{B}$-field and the Poynting vector $\mathbf{S}$ as dynamical variables, and cast their evolution equations in conservation form [29, 30]. The force-free constraints then become $\mathbf{S}\cdot\mathbf{B} = 0$ and $S^2 < B^4$ [30]. An advantage of this formulation is that it can be easily embedded into an ideal GRMHD code [29]. The GRFF formulation adopted here is identical to [29], except that at every timestep, in addition to $S^2 < B^4$, we also enforce the algebraic constraint $\mathbf{S}\cdot\mathbf{B} = 0$, which was ignored in [29]. For a discussion of possible shortcomings of this corrective enforcement of the force-free conditions see [29, 31]. This formulation is embedded in the fully GRMHD infrastructure presented and tested in [32–34]. Moreover, to enforce the $\nabla\cdot\mathbf{B} = 0$ constraint on our adaptive-mesh-refinement grids, the magnetic induction equation is evolved via the vector potential formulation introduced in [12, 33, 34], coupled to the Generalized Lorenz (GL) gauge condition [13, 34, 35], with damping parameter $\xi = 1.5/\Delta t$, where Δt is the coarsest level's timestep.

At large separations, the inspiral timescale is much longer than the orbital timescale. So to model the BHNS spacetime and the NS matter fields, we adopt quasiequi-

* Also at Department of Astronomy and NCSA, University of Illinois at Urbana-Champaign, Urbana, IL 61801

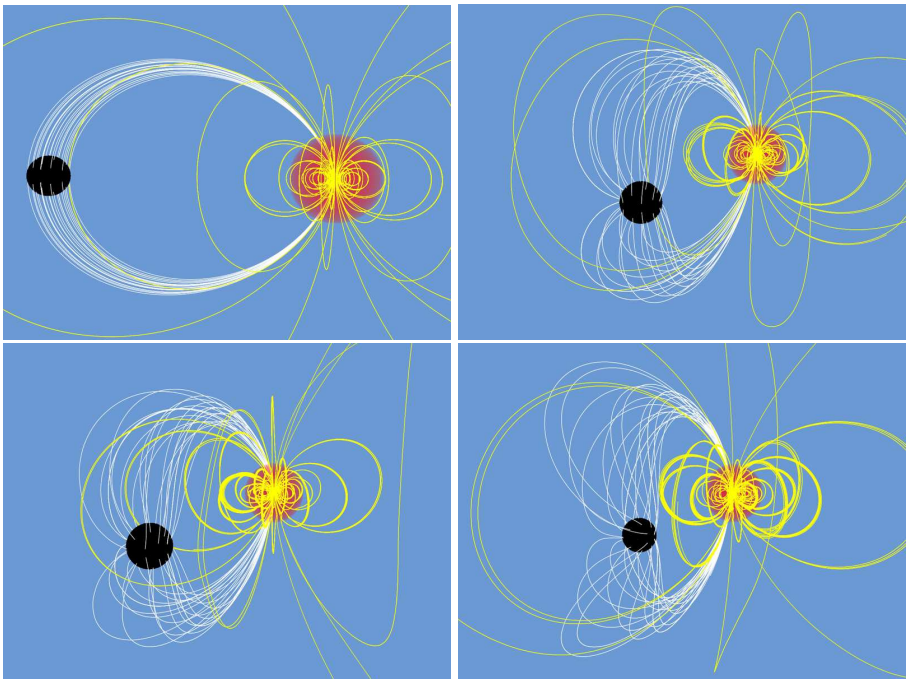

FIG. 1. Initial magnetic field in the $a_* = 0$ case (upper left panel). Relaxed magnetic field at $t \approx 1.5$ orbits: $a_* = 0$ (lower left panel), $a_* = -0.5$ (upper right panel), and $a_* = 0.75$ (lower right panel). The black sphere represents the BH horizon and the NS is shown in red. Both white and yellow lines are the magnetic fields lines. White lines distinguish field lines that intersect the BH horizon.

librium solutions of the conformal-thin-sandwich (CTS) equations for companions at fixed orbital separation [5, 36, 37]. The CTS approximation is excellent at the separations and BH spins considered here, yielding a binary spacetime with a helical Killing vector. In such a spacetime the matter and gravitational fields are stationary in the corotating frame of the binary, enabling us to perform the simulations in the center-of-mass frame by simply rotating the metric, as well as the fluid rest-mass density and four-velocity, following [38]. This reduces the problem to evolving the EM fields ($\mathbf{B}$ and $\mathbf{S}$) in the background matter fields and spacetime.

Given that force-free electrodynamics is a limit of ideal MHD, the *same* ideal MHD evolution equations can be used to evolve both the NS interior and the force-free exterior EM fields, provided in the exterior a compatible force-free velocity is used [29] and the rest-mass density is set to zero. This guarantees a smooth transition from the ideal MHD interior to the force-free exterior, and the MHD variables on the NS surface effectively provide boundary conditions for the exterior force-free evolution. However, given that the chosen initial A-field is not a CTS solution, we evolve the induction equation [Eqs. (8), (9) in [12]] in the NS interior, using the known CTS fluid four-velocity. This sets the boundary condition on the NS surface for the Poynting vector and magnetic field in the exterior. For more details see [30]. An alternative scheme for matching the interior ideal MHD to the exterior force-free regime was introduced in [39].

After tidal disruption, a GRFF treatment becomes inadequate and must be replaced by full GRMHD. Furthermore, according to [40–42] the ideal MHD approximation may break down in the regions near the surface. This motivates a resistive GRMHD simulation with realistic conductivity, including cooling. However, here we take the widely adopted approach of neglecting the magnetic field backreaction onto the NS matter (e.g. [31, 39, 43]), which likely becomes important in a region in the outer layers of the NS, and assume ideal MHD throughout. Preliminary resistive MHD studies of rotating neutron stars in [22], which include the effects EM backreaction onto the NS matter, show that the outgoing EM luminosity is within 20% of the values obtained in [31], which neglect the EM backreaction onto the matter. Thus, we expect the error of neglecting the EM backreaction to be of this order magnitude at most.

In addition to our new GRFF evolution techniques, we have also added two equivalent diagnostics to monitor the outgoing EM luminosity: (i) the ϕ_2 Newman-Penrose scalar [44–46], and (ii) the Poynting vector $\mathbf{S} = (\mathbf{E} \times \mathbf{B})/4\pi$. To compute ϕ_2 we use the same null tetrad as in [47], and the outgoing luminosity is [48]

$$L_{\rm EM} \equiv \lim_{r\to\infty} \frac{1}{4\pi} \int r^2 |\phi_2|^2 d\Omega = \lim_{r\to\infty} \int r^2 S^{\hat{r}} d\Omega. \quad (1)$$

The spacetime and NS initial data we use correspond to cases A, B, C in Table I in [5]. The BH spin parameters are $a_* \equiv a/M_H = -0.5, 0, 0.75$, and the BH:NS mass ratio is $q = 3$. The NS fluid is modeled as an equilibrium, irrotational, unmagnetized, $\Gamma = 2$ polytrope. We seed

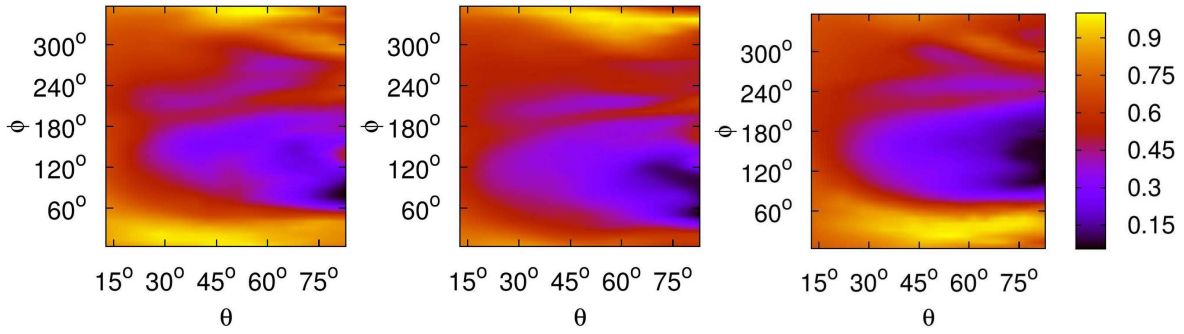

FIG. 2. Angular distribution of Poynting flux, normalized by its peak value on a sphere of radius $120M = 915(M_{\rm NS}/1.4M_\odot)$km. Left: spin -0.5, middle: spin 0, right: spin 0.75. The plots correspond to a time after ~ 2 orbits. The azimuthal (ϕ) and polar (θ) angles are defined with respect to a spherical coordinate system centered on the center of mass of the binary.

the initial NS with a purely poloidal magnetic field that approximately corresponds to that generated by a current loop. The coordinate-basis toroidal component of this vector potential is

$$A_\phi = \frac{\pi r_0^2 I_0}{(r_0^2+r^2)^{3/2}}\left(1+\frac{15 r_0^2(r_0^2+\varpi^2)}{8(r_0^2+r^2)^2}\right), \qquad (2)$$

where r_0 is the current loop radius, I_0 the loop current, $r^2=(x-x_{\rm NS})^2+(y-y_{\rm NS})^2+z^2$, $\varpi^2=(x-x_{\rm NS})^2+(y-y_{\rm NS})^2$, and $x_{\rm NS}, y_{\rm NS}$ are the initial coordinates of the NS center of mass. For $r_0 \ll r$ Eq. (2) gives rise to the standard B-field from a current loop on the z-axis, and the characteristic $1/r^3$ fall-off of a standard magnetic dipole on the $z=0$ plane. Choosing $r_0 = R_{\rm NS}/3$ in all our simulations, where $R_{\rm NS}$ is the NS polar radius, we find that the initial magnetic field scales as $1/r^3$ outside the NS to a very good degree. Our simulations scale with $|B|$. If we set $I_0 = 0.0007$, the initial NS polar magnetic field (as measured by a CTS normal observer) is 8.8×10^{15}G. The initial B-field geometry is shown in the upper left panel of Fig. 1. To set the initial electric field, we first set the matter velocity u_i in the interior according to the CTS solution, and set the exterior u_i to 0 except for the perpendicular component to the B-field, which falls-off as $1/r^2$ from its NS surface value. The E-field is then computed using the ideal MHD condition. These initial data satisfy the force-free conditions.

For $a_*=0$ we perform a resolution study: the low, medium and high resolutions cover, $R_{\rm BH}$, the BH apparent horizon ($R_{\rm NS}$, the NS minimum) radius by 19, 29, 36 (39, 60, 75) zones, respectively. The resolutions used for $a_*\neq 0$ correspond to the high-resolution $a_*=0$ run. In all simulations we use 9 levels of refinement with two sets of nested boxes, differing in size by factors of 2, and each centered onto one of the orbiting stars. The finest box around the BH (NS) has a side length $4.8R_{\rm BH}$ ($2.4R_{\rm NS}$). We place the outer boundary at $400M \approx 3050(M_{\rm NS}/1.4M_\odot)$km, and impose reflection symmetry across the orbital plane.

After a transient phase lasting a little over 1 orbit, the B-field settles into a quasistationary configuration shown in Fig. 1. It is evident that for $a_*\neq 0$ partial winding of the magnetic field has taken place due to frame dragging, which is most prominent for $a_*=0.75$.

In Fig. 2 we show the angular distribution of the Poynting flux. In all cases, it peaks within a broad beam of $\sim 40^\circ$ in the azimuthal direction, and in the $a_*=0$ and $a_*=0.75$ cases within $\sim 60^\circ$ from the orbital plane. This may establish a lighthouse effect as a characteristic EM signature of BHNS systems prior to merger, if the variation is not washed out by intervening matter. The distribution of the flux on a sphere far away from the binary, settles down to an approximately stationary state in a frame corotating with the binary.

The time evolution of the computed luminosities is shown in Fig. 3. After a transient period caused by our choice of non-stationary initial magnetic fields, the luminosities settle to an approximately constant value as expected. We find that the time-averaged luminosities after the first 1.5 orbits at the adopted separation are

$$\begin{aligned}
\langle L_{a_*=-0.5}\rangle &= 6.6\times10^{42}\left(\frac{B_{\rm NS,p}}{10^{13}{\rm G}}\right)^2\left(\frac{M_{\rm NS}}{1.4M_\odot}\right)^2 {\rm erg/s},\\
\langle L_{a_*=0}\rangle &= 6.2\times10^{42}\left(\frac{B_{\rm NS,p}}{10^{13}{\rm G}}\right)^2\left(\frac{M_{\rm NS}}{1.4M_\odot}\right)^2 {\rm erg/s},\\
\langle L_{a_*=0.75}\rangle &= 4.8\times10^{42}\left(\frac{B_{\rm NS,p}}{10^{13}{\rm G}}\right)^2\left(\frac{M_{\rm NS}}{1.4M_\odot}\right)^2 {\rm erg/s},
\end{aligned} \qquad (3)$$

where $B_{\rm NS,p}$ is the NS polar magnetic field strength measured by a CTS normal observer, and $M_{\rm NS}$ is the NS rest mass. As the B-field does not feed back onto the matter evolution, the EM luminosity scales exactly as B^2. The characteristic frequency of this EM radiation is of order the orbital frequency $\sim 200(M_{\rm NS}/1.4M_\odot)^{-1}$Hz at the adopted separation, and hence smaller than typical interstellar-medium plasma frequencies $\sim$ 9kHz. Thus, this radiation will be reprocessed before it reaches the observer.

We now compare our results to the approximate UI formula. The Poynting luminosity of a BHNS UI in the large q limit is given by [18]

$$L_{\rm UI} = \frac{8}{\pi}\left(\frac{r_H}{2M_H}\right)^2 v_{\rm rel}^2 \bar{B}_{\rm NS,p}^2\left(\frac{R_{NS}}{r}\right)^6 q^2 M_{\rm NS}^2 \qquad (4)$$

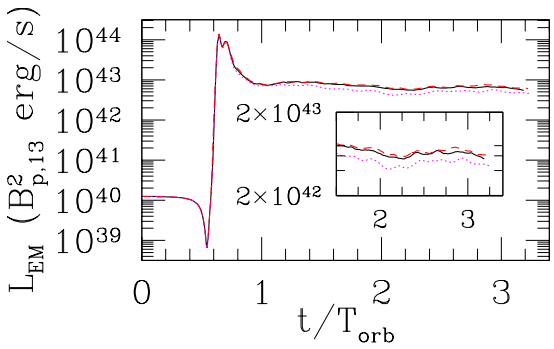

FIG. 3. Poynting luminosity vs time calculated on a sphere of radius $120M = 915(M_{\rm NS}/1.4M_\odot)$km for all 3 cases: $a_* = -0.5$ (red) dashed line, $a_* = 0$ (black) solid line, $a_* = 0.75$ (magenta) dotted line. The inset focuses on the last 1.7 orbits of evolution. Here $B_{p,13} = B_{\rm NS,p}/10^{13}$G and $T_{\rm orb}$ is the orbital period.

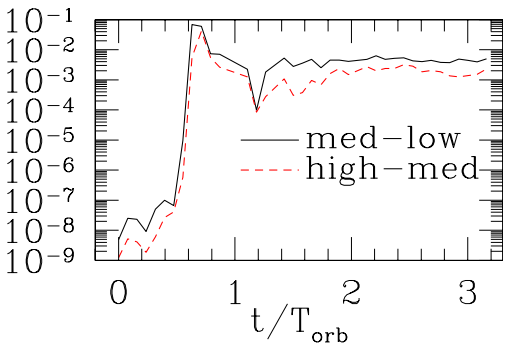

FIG. 4. Convergence of EM luminosity normalized by the maximum luminosity vs. time. The difference between high and medium resolutions is smaller than that between medium and low resolutions, indicating that our scheme is convergent.

where r_H is the horizon radius in units of the BH mass M_H, $\bar{B}_{\rm NS,p}$ is the NS polar magnetic field as measured by zero-angular-momentum observers (ZAMOs) [49], i.e., normal observers in a Kerr spacetime in Boyer-Lindquist coordinates, and r is the binary separation. Here $v_{\rm rel}$ is the azimuthal velocity of magnetic field lines as measured by ZAMOs, for which the following relation was proposed [18]: $v_{\rm rel} = r(\Omega - \Omega_{\rm NS}) - \frac{a}{4\sqrt{2}}$, where Ω is the orbital angular frequency, and $\Omega_{\rm NS}$ is the NS spin angular frequency. As our BHNS binaries are irrotational, we set $\Omega_{\rm NS} = 0$. Using the binary parameters from our simulations and setting $\bar{B}_{\rm NS,p} \approx B_{\rm NS,p}$ in Eq. (4), we find

$$\begin{aligned} L_{{\rm UI},a_*=0.75} &= 0.12\langle L_{a_*=0.75}\rangle, \\ L_{{\rm UI},a_*=0} &= 0.5\langle L_{a_*=0}\rangle, \\ L_{{\rm UI},a_*=-0.5} &= 0.7\langle L_{a_*=-0.5}\rangle. \end{aligned} \tag{5}$$

Thus, the UI formula seems to predict well the overall magnitude of our computed luminosities. However, in contrast to Eq. (5), which predicts that $L_{{\rm UI},a_*=-0.5}/L_{{\rm UI},a_*=0} \approx 1.5$ and $L_{{\rm UI},a_*=-0.5}/L_{{\rm UI},a_*=0.75} \approx 7.8$, (3) show only a weak dependence of the Poynting luminosity on the BH spin. This is likely due in part to the spin dependence being added linearly in the proposed formula for $v_{\rm rel}$, and in part to the existence of magnetic dipole emission.

In addition to the UI luminosity, another important EM radiation emission mechanism, that always operates, is that due to the accelerating MD moment of the NS. The approximate MD luminosity is given by [25]

$$\begin{aligned} L_{\rm EM,MD} \approx 2.4\times10^{41}&\left(\frac{v}{0.3c}\right)^2\left(\frac{B_{\rm NS,p}}{10^{13}{\rm G}}\right)^2 \\ &\left(\frac{M_{\rm NS}}{1.4M_\odot}\right)^2\left(\frac{r}{6.6R_{\rm NS}}\right)^{-6}{\rm erg/s}, \end{aligned} \tag{6}$$

where we inserted parameters from our simulations. $L_{\rm EM,MD}$ is only ~ 20 times smaller than what we observe in our simulations, but is included in our calculated luminosity (see also [22]). MD emission dominates when UI ceases due to corotation (and $a_* = 0$ for BHNSs) or $\zeta_\phi > 1$, which may be the case for NSNS binaries [23].

The results of our resolution study for $a_* = 0$ are shown in Fig. 4, where it is demonstrated that our scheme is convergent, and that the resulting luminosities in the two highest resolutions agree to within $\sim 5\%$. Due to numerical resistivity, the EM energy in the NS interior is conserved after 3 orbits to within 10%, 11%, 7% in the $a_* = -0.5$, $a_* = 0$, $a_* = 0.75$ cases, respectively. Thus, these errors should be taken as the approximate error bars of our calculations. Our convergence test also shows that the numerical dissipation decreases toward zero, but the outgoing radiation converges to a nonzero value, with increasing resolution. Also, freezing the spacetime and matter evolution, while evolving the EM fields shows that the outgoing Poynting flux is 4 orders of magnitude smaller than the values in Eq. (3). Thus, the measured luminosities are not corrupted by interior energy leaking to the exterior. Calculating the ratio of the electric flux to the initial magnetic flux through a hemisphere of radius $1.5R_{\rm NS}$ centered on the NS vs time, we find this ratio to be $< 10^{-3}$. Furthermore, we performed the low-resolution run of the nonspinning BH case, setting the initial exterior E-field and u_i to 0. In this case we expect $\int \mathbf{E}\cdot d\mathbf{S} = 0$. We calculated the ratio $\int \mathbf{E}\cdot d\mathbf{S}/\int |E| dS$, which quantifies how close to 0 $\int \mathbf{E}\cdot d\mathbf{S}$ is, and have found it to be $< 1\%$ at all times. These two results indicate that little spurious charge is generated in our simulations. Moreover, calculating the Poynting luminosity in this last run, we find the same values [within 1% (0.1%) following the first (second) orbit] as in the case where the initial exterior u_i continuously falls off as $1/r^2$ from its value on the NS surface. Thus, the relaxed solution we obtain is nearly independent of these initial configurations.

In a future work we plan to extend our simulations to study the variation of the outgoing Poynting luminosity during the inspiral phase, and its dependence on different mass ratios.

ACKNOWLEDGMENTS

The authors wish to thank Charles F. Gammie, Roman Gold, and Yuk Tung Liu for useful discussions. We also thank the Illinois Relativity Group's REU team [Gregory Colten, Albert Kim, Brian Taylor, and Francis Walsh] for assistance in producing Fig. 1. These visualizations were created using the ZIB Amira software package [50], and we gratefully acknowledge the Zuse Institute Berlin for providing us a license. This paper was supported in part by NSF Grants AST-1002667, and PHY-0963136 as well as NASA Grant NNX11AE11G at the University of Illinois at Urbana-Champaign. This work used the Extreme Science and Engineering Discovery Environment (XSEDE), which is supported by NSF grant number OCI-1053575.

[1] B. Abbott and the LIGO Scientific Collaboration, Phys. Rev. D **77**, 062002 (Mar. 2008).

[2] D. A. Brown, S. Babak, P. R. Brady, N. Christensen, T. Cokelaer, J. D. E. Creighton, S. Fairhurst, G. Gonzalez, E. Messaritaki, B. S. Sathyaprakash, P. Shawhan, and N. Zotov, Class. Quant. Grav. **21**, S1625 (Oct. 2004).

[3] V. Kalogera, K. Belczynski, C. Kim, R. O'Shaughnessy, and B. Willems, Phys. Rept. **442**, 75 (Apr. 2007).

[4] J. Abadie, B. P. Abbott, R. Abbott, M. Abernathy, T. Accadia, F. Acernese, C. Adams, R. Adhikari, P. Ajith, B. Allen, and et al., Classical and Quantum Gravity **27**, 173001 (Sep. 2010).

[5] Z. B. Etienne, Y. T. Liu, S. L. Shapiro, and T. W. Baumgarte, Phys. Rev. D **79**, 044024 (Feb. 2009).

[6] M. D. Duez, F. Foucart, L. E. Kidder, C. D. Ott, and S. A. Teukolsky, Class.Quant.Grav. **27**, 114106 (2010), arXiv:0912.3528 [astro-ph.HE].

[7] F. Foucart, M. D. Duez, L. E. Kidder, and S. A. Teukolsky, Phys.Rev. **D83**, 024005 (2011), arXiv:1007.4203 [astro-ph.HE].

[8] K. Kyutoku, H. Okawa, M. Shibata, and K. Taniguchi, Phys.Rev. **D84**, 064018 (2011), arXiv:1108.1189 [astro-ph.HE].

[9] B. D. Lackey, K. Kyutoku, M. Shibata, P. R. Brady, and J. L. Friedman, Phys.Rev. **D85**, 044061 (2012), arXiv:1109.3402 [astro-ph.HE].

[10] F. Foucart, M. B. Deaton, M. D. Duez, L. E. Kidder, I. MacDonald, *et al.*(2012), arXiv:1212.4810 [gr-qc].

[11] G. Lovelace, M. D. Duez, F. Foucart, L. E. Kidder, H. P. Pfeiffer, *et al.*(2013), arXiv:1302.6297 [gr-qc].

[12] Z. B. Etienne, Y. T. Liu, V. Paschalidis, and S. L. Shapiro, Phys. Rev. D **85**, 064029 (Mar. 2012).

[13] Z. B. Etienne, V. Paschalidis, and S. L. Shapiro, Phys. Rev. D **86**, 084026 (Oct. 2012), arXiv:1209.1632 [astro-ph.HE].

[14] S. Nissanke, M. Kasliwal, and A. Georgieva(2012), arXiv:1210.6362 [astro-ph.HE].

[15] P. Goldreich and W. H. Julian, Astrophys. J. **157**, 869 (Aug. 1969).

[16] P. Goldreich and D. Lynden-Bell, Astrophys. J. **156**, 59 (Apr. 1969).

[17] S. D. Drell, H. M. Foley, and M. A. Ruderman, Journal of Geophysical Research **70**, 3131 (Jul. 1965).

[18] S. T. McWilliams and J. Levin, Astrophys. J. **742**, 90 (Dec. 2011), arXiv:1101.1969 [astro-ph.HE].

[19] M. Lyutikov, Phys.Rev. **D83**, 124035 (2011), arXiv:1104.1091 [astro-ph.HE].

[20] D. J. D'Orazio and J. Levin, ArXiv e-prints(Feb. 2013), arXiv:1302.3885 [astro-ph.HE].

[21] A. L. Piro, Astrophys. J. **755**, 80 (Aug. 2012), arXiv:1205.6482 [astro-ph.HE].

[22] C. Palenzuela, L. Lehner, M. Ponce, S. L. Liebling, M. Anderson, *et al.*(2013), arXiv:1301.7074 [gr-qc].

[23] D. Lai, Astrophys. J. Lett. **757**, L3 (Sep. 2012), arXiv:1206.3723 [astro-ph.HE].

[24] B. M. Hansen and M. Lyutikov, Mon.Not.Roy.Astron.Soc. **322**, 695 (2001), arXiv:astro-ph/0003218 [astro-ph].

[25] K. Ioka and K. Taniguchi, Astrophys.J.(2000), arXiv:astro-ph/0001218 [astro-ph].

[26] S. Komissarov, Mon.Not.Roy.Astron.Soc. **336**, 759 (2002), arXiv:astro-ph/0202447 [astro-ph].

[27] C. Palenzuela, T. Garrett, L. Lehner, and S. L. Liebling, Phys. Rev. D **82**, 044045 (Aug. 2010), arXiv:1007.1198 [gr-qc].

[28] J. C. McKinney and C. F. Gammie, Astrophys.J. **611**, 977 (2004), arXiv:astro-ph/0404512 [astro-ph].

[29] J. C. McKinney, Mon. Not. Roy. Astron. Soc. **367**, 1797 (Apr. 2006), arXiv:astro-ph/0601410.

[30] V. Paschalidis, B. E. Zachariah, and L. S. Shapiro, In preparation(2013).

[31] A. Spitkovsky, Astrophys.J. **648**, L51 (2006), arXiv:astro-ph/0603147 [astro-ph].

[32] M. D. Duez, Y. T. Liu, S. L. Shapiro, and B. C. Stephens, Phys.Rev. **D72**, 024028 (2005), arXiv:astro-ph/0503420 [astro-ph].

[33] Z. B. Etienne, Y. T. Liu, and S. L. Shapiro, Phys.Rev. **D82**, 084031 (2010), arXiv:1007.2848 [astro-ph.HE].

[34] Z. B. Etienne, V. Paschalidis, Y. T. Liu, and S. L. Shapiro, Phys. Rev. D **85**, 024013 (Jan. 2012).

[35] B. D. Farris, R. Gold, V. Paschalidis, Z. B. Etienne, and S. L. Shapiro, Phys.Rev.Lett. **109**, 221102 (2012), arXiv:1207.3354 [astro-ph.HE].

[36] K. Taniguchi, T. W. Baumgarte, J. A. Faber, and S. L. Shapiro, Phys.Rev. **D72**, 044008 (2005), arXiv:astro-ph/0505450 [astro-ph].

[37] T. W. Baumgarte and S. L. Shapiro, *Numerical Relativity: Solving Einstein's Equations on the Computer* (Cambridge University Press, 2010).

[38] B. D. Farris, Y. T. Liu, and S. L. Shapiro, Phys.Rev. **D84**, 024024 (2011), arXiv:1105.2821 [astro-ph.HE].

[39] L. Lehner, C. Palenzuela, S. L. Liebling, C. Thompson, and C. Hanna, ArXiv e-prints(Dec. 2011), arXiv:1112.2622 [astro-ph.HE].

[40] L. Mestel and S. Shibata, Mon. Not. Roy. Astron. Soc. **271**, 621 (Dec. 1994).

[41] I. Contopoulos, D. Kazanas, and C. Fendt, Astrophys. J. **511**, 351 (Jan. 1999), arXiv:astro-ph/9903049.

[42] Y. Mizuno, Astrophys. J. Supp. **205**, 7 (Mar. 2013), arXiv:1301.6052 [astro-ph.HE].
[43] A. Gruzinov, Phys.Rev.Lett. **94**, 021101 (2005), arXiv:astro-ph/0407279 [astro-ph].
[44] E. Newman and R. Penrose, Journal of Mathematical Physics **3**, 566 (May 1962).
[45] S. A. Teukolsky, Astrophys.J. **185**, 635 (1973).
[46] C. Palenzuela, T. Garrett, L. Lehner, and S. L. Liebling, Phys.Rev. **D82**, 044045 (2010), arXiv:1007.1198 [gr-qc].
[47] P. Moesta, D. Alic, L. Rezzolla, O. Zanotti, and C. Palenzuela, Astrophys.J. **749**, L32 (2012), arXiv:1109.1177 [gr-qc].
[48] Notice the factor of $1/4\pi$, which was omitted in [47]. This factor results from the choice of null tetrad. A similar factor of $1/2\pi$ was used in the $L_{\rm EM}$ formulae reported in [45, 46] where a different null tetrad was used.
[49] K. S. Thorne, R. H. Price, and D. A. MacDonald, *Black Holes: The Membrane Paradigm* (1986).
[50] D. Stalling, M. Westerhoff, and H.-C. Hege, in *The Visualization Handbook; Amira: A Highly Interactive System for Visual Data Analysis*, edited by C. D. Hansen and C. R. Johnson (Elsevier, 2005) Chap. 38, pp. 749–767, ISBN 978-0-12-387582-2.